Chemosphere 183 (2017) 323–331

Contents lists available at ScienceDirect

Chemosphere

journal homepage: www.elsevier.com/locate/chemosphere

Electromagnetic induction of foam-based nanoscale zerovalent iron (NZVI) particles to thermally enhance non-aqueous phase liquid (NAPL) volatilization in unsaturated porous media: Proof of concept

Supawan Srirattana [a, b], Kitsanateen Piaowan [a, b], Gregory V. Lowry [c, d], Tanapon Phenrat [a, b, *]

[a] Research Unit for Integrated Natural Resources Remediation and Reclamation (IN3R), Department of Civil Engineering, Faculty of Engineering, Naresuan University, Phitsanulok, 65000, Thailand
[b] Center of Excellence for Sustainability of Health, Environment and Industry (SHEI), Faculty of Engineering, Naresuan University, Phitsanulok, 65000, Thailand
[c] Center for Environmental Implications of Nanotechnology (CEINT), Carnegie Mellon University, Pittsburgh, PA 15213-3890, USA
[d] Department of Civil & Environmental Engineering, Carnegie Mellon University, Pittsburgh, PA 15213-3890, USA

HIGHLIGHTS

- This study uses F-NZVI with a LF-EMF to thermally enhanced trichloroethylene evaporation in unsaturated porous media.
- F-NZVI generates heat under the LF-EMF and increases the TCE evaporation by 40 times compared to the case without the LE-EMF.
- Using F-NZVI together with LF-EMF requires much lower irradiation frequency (336 times lower) that radio frequency heating.

GRAPHICAL ABSTRACT

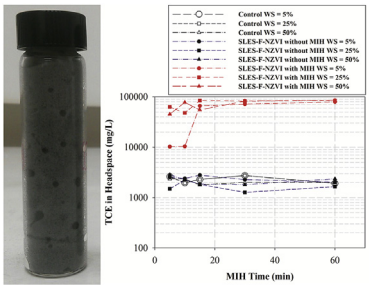

ARTICLE INFO

Article history:
Received 4 January 2017
Received in revised form
30 March 2017
Accepted 19 May 2017
Available online 20 May 2017

Handling Editor: Min Jang

Keywords:
Nanoscale zerovalent iron particles
Foam
Unsaturated porous media
Magnetic induction heating
Chlorinated volatile organic compounds
Dense non-aqueous phase liquid (DNAPL)

ABSTRACT

Nanoscale zerovalent iron (NZVI) is a promising remediation agent for volatile organic compound (VOC) contamination in saturated sub-surfaces, but is rarely applied to the vadose zone as there are not enough water molecules in the unsaturated zone to participate in reductive dechlorination. In this study, we evaluated the possibility of using foam as a carrying vehicle to emplace NZVI in unsaturated porous media followed by the application of low frequency-electromagnetic field (LF-EMF) to enhance VOC volatilization in laboratory batch reactors. We found that the optimal condition for generating foam-based NZVI (F-NZVI) was using sodium lauryl ether sulfate (SLES) at a concentration of 3% (w/w) and a N_2 flow rate of 500 mL/min. Also, F-NZVI could carry as much as 41.31 g/L of NZVI in the liquid phase of the foam and generate heat to raise ΔT to 77 °C in 15 min under an applied LF-EMF (150 kHz and 13 A). Under these conditions, F-NZVI together with LF-EMF enhanced trichloroethylene (TCE) volatilization from TCE-dense non-aqueous phase liquid (DNAPL) in unsaturated sand by 39.51 ± 6.59-fold compared to reactors without LF-EMF application. This suggested that using F-NZVI together with LF-EMF could theoretically be an alternative to radio frequency heating (RFH) as it requires a much lower irradiation frequency (336-fold lower), which should result in significantly lower capital and operational costs compared to RFH.

* Corresponding author. Research Unit for Integrated Natural Resources Remediation and Reclamation (IN3R), Department of Civil Engineering, Faculty of Engineering, Naresuan University, Phitsanulok, 65000, Thailand.
E-mail address: pomphenrat@gmail.com (T. Phenrat).

http://dx.doi.org/10.1016/j.chemosphere.2017.05.114
0045-6535/

Abbreviations

CVOC	Chlorinated volatile organic compound
DNAPL	Dense non-aqueous phase liquid
EM	Electromagnetic
ERH	Electrical resistance heating
EMFG	Electromagnetic field generator
F-NZVI	Foam-based nanoscale zerovalent iron
LF-EMF	Low frequency-electromagnetic field
MIH	Magnetic induction heating
MWH	Microwave heating
PV	Pore volume
RFH	Radio frequency heating
SLES	Sodium lauryl ether sulfate
SVE	Soil vapor extraction
TCE	Trichloroethylene
VOC	Volatile organic compound
WS	Water saturation; w/w Weight by weight

Nomenclatures

ε_0	Permittivity of free space (8.85×10^{-12} F/m)
ε''_{eff}	Effective imaginary permittivity (unit less)
$\|E\|$	Magnitude of the applied electric field (V/m)
f	Frequency (Hz)
k_{HI}	Heat induction rate constant (1/min)
I	Current (A)
$Mass_{NZVI}$	Mass of NZVI (g)
$P_{cr\text{-}foam}$	Critical capillary pressure of foam destruction (Pa)
P_{EM}	Power dissipated by EM heating (W)
P_{MIH}	Power dissipated by MIH (W)
P_{RFH}	Power dissipated by RFH (W)
ΔT	Temperature change (°C)
ΔT_{max}	Maximum induced temperature (°C)
θ_{cr}	Critical moisture content (Unit less)
ΔU	Area under hysteresis curve (emu/g G)

1. Introduction

Vadose zone contamination with chlorinated volatile organic compounds (CVOCs) is a persistent and vexing environmental problem, jeopardizing environmental quality and public health. CVOCs may be entrapped as dense non-aqueous phase liquid (DNAPL) residuals in pores within the vadose zone and behave as long-term sources of toxic vapor that migrates to the land surface and into buildings, causing vapor intrusion problems (Ronen et al., 2004; Abreu and Johnson, 2005; Brusseau et al., 2013). Additionally, DNALs in the vadose zone serve as long-term origins of groundwater contamination by discharging CVOCs to underlying groundwater via infiltration and percolation (Rosenbloom et al., 1993; Soga et al., 2003). While cleaning a CVOC-contaminated saturated zone is comprised by a variety of remedial alternatives, remediation techniques for CVOCs from the vadose zone are limited to excavation, soil vapor extraction (SVE) (Yang et al., 2001; Yoon et al., 2003), and bioventing (Boulding and Ginn, 2003; Brusseau et al., 2013).

SVE, the most commonly applied VOC vadose zone remediation technique, relies on extracting VOCs in the soil vapor phase. Nevertheless, at *in situ* natural temperatures, its removal efficacy is limited by mass transfer based on slow desorption and protracted diffusion of VOCs from the soil matrix, especially if less permeable layers exist (Werth and Reinhard, 1997; Heron et al., 1998). Thermal-enhanced options (Werth and Reinhard, 1997; Poppendieck et al., 1999a,b; Price et al., 1999; Nakamura et al., 2000; Vermeulen and McGee, 2000; Roland et al., 2008; Truex et al., 2009) have received increasing attention in recent years as they are able to increase vapor pressure to overcome the mass transfer limitations of SVE. Electrical heating, such as electrical resistance heating (ERH), and electromagnetic heating, like radio frequency heating (RFH) and microwave heating (MWH), are novel thermal alternatives that surmount these types of technical problems (Heron et al., 1998; Price et al., 1999; Vermeulen and McGee, 2000). ERH was reported to remove CVOCs by as much as 98% in water-saturated soil after a 175-day field-scale test (Beyke and Fleming, 2005). Similarly, RFH was also described to achieve similar removal efficiency in water-saturated soil (Smith and Hinchee, 1993). Electromagnetic (EM) heating, which includes RFH and MWH, utilizes the conversion of EM energy into thermal energy through the interaction between the EM field and the atoms or molecules present in the irradiated material. Thus, this interaction is governed by the nature of the irradiated material and radiation frequency. RFH and MWH employ frequencies as high as 500 MHz (Lowe et al., 1999; Price et al., 1999) and even up to 500 GHz (Lowe et al., 1999; Falciglia et al., 2013), respectively.

While only conduction and dielectric loss are considered primarily responsible for the RFH of soil, magnetic loss is another heating mechanism capable of operating at lower frequency and, hence, theoretically capable of reducing transmission losses and capitals cost of EMF-generating equipment. Magnetic induction heating (MIH) takes place through hysteresis loss of magnetic materials because of the irreversible magnetization of an EMF. At a particular EMF frequency (f), the amount of power dissipated by MIH (P_{MIH}) (W) can be expressed as (Li et al., 2010):

$$P_{MIH} = f\Delta U, \quad (1)$$

where ΔU is the area under the hysteresis curve influenced by the characteristics of the magnetic materials. The degree of irreversibility, ΔU, is related to the amount of energy dissipation upon the reversal of the field. For this reason, ferromagnetic nanoparticles, such as nanoscale zerovalent iron (NZVI), are promising remediation agents (Tratnyek and Johnson, 2006; He et al., 2007; Phenrat et al., 2007, 2008, 2009b; Berge and Ramsburg, 2010; He et al., 2010; Phenrat et al., 2010b, 2011a, 2011b; O'Carroll et al., 2013; Kocur et al., 2015; Phenrat et al., 2015), and can be coupled with LF-EMF to function as a combined remediation method to elevate the rate and completeness of an *in situ* cleaning of CVOCs at the subsurface. Although there has been more of focus on using the magnetic properties of ZVI for environmental treatment, there has indeed been application of magnetic treatments to enhance the corrosion of ZVI, increasing the reaction rate or pollutant removal efficacy (Liang et al., 2014a, 2014b; Xu et al., 2016). Recently, in terms of subsurface remediation, Phenrat's group employed MIH to thermally enhance remediation. They revealed that using ZVI and NZVI with applied LF-EMF enhanced dechlorination of dissolved TCE and TCE in a soil-water-TCE system up to 5-fold compared to the absence of LF-EMF, presumably from magnetically accelerated

ZVI corrosion and thermally-enhanced desorption of TCE from soil (Phenrat et al., 2016). Similarly, Phenrat and Kumloet utilized polyelectrolyte-modified NZVI together with LF-EMF to improve the degradation of TCE- and PCE-DNAPL. With four cycles of LF-EMF application, polymer-modified NZVI-induced heat elevates the temperature up to 87 °C and increases the rate constants of TCE-DNAPL and PCE-DNAPL up to 14.58- and 58.01-fold, respectively, versus the dechlorination rate without LF-EMF (Phenrat and Kumloet, 2016).

In the same vein, NZVI is thought to be lead to heat under applied LF-EMF in the vadose zone just as it does in the saturated zone (Phenrat and Kumloet, 2016; Phenrat et al., 2016). Conceptually, along with SVE, the heat generated by NZVI with LF-EMF should speed up CVOC removal in the vadose zone via thermally-enhanced volatilization (Fig. S1 in the Supporting Information (SI)). Raising the chemical vapor pressures by heating soil *in situ* can diminish the remediation time like RFH, but at a lower frequency, resulting in a less complicated and more economic system and operation. Nevertheless, NZVI must be placed in the vadose zone. Recent studies by Zhong and Li's group proposed using foam-assisted delivery of NZVI in the vadose zone (Zhong et al., 2010; Shen et al., 2011; Ding et al., 2013) to overcome the technical difficulty of delivering water-based NZVI dispersion to the vadose zone, which may cause unintended CVOC dissolution and migration to underlying aquifers. Foaming surfactant has recently gained much consideration as a foam-based soil flushing procedure (Zhao et al., 2016) to remove pesticides (Wang et al., 2015), polychlorinated biphenyl (Wang and Chen, 2012), and CVOCs (Jeong et al., 2000; Maire and Fatin-Rouge, 2017) from unsaturated porous media. Therefore, theoretically, foam-based NZVI can perform two remediation processes: 1) flushing CVOC from the soil; and 2) leaving behind NZVI for electromagnetic induction heating.

The present study evaluated the feasibility of using foam-based NZVI (F-NZVI) together with LF-EMF (150 kHz) to enhance TCE volatilization from a TCE-DNAPL in laboratory-scaled unsaturated porous media. The greater the enhanced TCE volatilization via MIH of F-NZVI, the more effective the thermally-enhanced SVE. Sodium lauryl ether sulfate (SLES) was used as a F-NZVI stabilizer. Magnetic characterization was conducted for NZVI and F-NZVI. Batch and column experiments were conducted to confirm F-NZVI stability and mobility in unsaturated porous media. The ability of F-NZVI to generate heat under an applied LF-EMF was also examined. TCE volatilization kinetics, both with and without LF-EMF, were compared to quantify the benefits of using LF-EMF together with F-NZVI. The feasibility of this combined remediation concept is discussed based on enhanced TCE evaporation and theoretical analysis of operational conditions between RFH without F-NZVI and MIH with F-NZVI to obtain similar energy dissipation.

2. Materials and methods

2.1. Chemicals and NZVI

TCE (>99.5%) was obtained from Aldrich (St. Louis, MO). SLES was used as a foam stabilizer in this study. NZVI was procured as Nanofer 25 (NF25) (Nanoiron, Czech Republic). Table S1 (in the SI) summarizes the physical properties of NF25 as gauged by the supplier. In addition, the magnetic properties of NZVI were characterized with a vibrational sample magnetometer (VSM).

2.2. F-NZVI generation procedure and characterization

The foam and F-NZVI generation procedure of this work was described in detail previously (Shen et al., 2011) and is outlined in the SI and Fig. S2. The quality of the control foam (no NZVI) and F-NZVI, foam stability, and bubble size distribution of the control foam and F-NZVI were determined as described in the SI (Mulligan and Eftekhari, 2003; Zhong et al., 2010). Each experiment was carried out in duplicate.

We determined the optimal F-NZVI generating conditions by assessing the optimal SLES concentration and N_2 flow rate. First, the optimal SLES concentration for foam generation was established with a N_2 flow rate of 125 mL/min at various surfactant concentrations of 1, 3, 5, 7, and 9% (w/w). Then, the optimal SLES dose was used to define the optimal N_2 flow rate by experimenting with various N_2 flow rates of 125, 300, and 500 mL/min with an NZVI concentration of 50 g/L. This optimal F-NZVI generation technique was further employed for other experiments in this study unless otherwise specified.

2.3. Delivery and placement of F-NZVI in the unsaturated sand-packed column

Prior to assessing the capability of LF-EMF and F-NZVI to accelerate TCE-DNAPL removal via electromagnetically induced volatilization, we first evaluated if F-NZVI could be delivered and placed in unsaturated porous media. The unsaturated sand-packed column used for this was a cylindrical acrylic column, 16 cm in length and 2 cm in inner diameter, packed with quartz sand with a grain size distribution between 0.45 and 0.85 mm as a simplified sand layer in vadose zone that could trap DNAPL residuals and thus target remediation with F-NZVI. The column was attached to the foam generation column (Fig. S2). 60 pore volumes (PVs) of F-NZVI generated the optimal SLES concentration and the optimal N_2 flow rate with NZVI concentration of 50 and 100 g/L being delivered into the unsaturated sand-packed column. Each experiment was conducted in duplicate. The breakthrough NZVI concentrations in F-NZVI were monitored. Furthermore, the concentration of NZVI deposited onto the unsaturated sand was established by dissecting the sand-packed column into eight 2-cm long segments. Further details surrounding the experimental setup are available in the SI.

2.4. Magnetic induction heating (MIH) of free F-NZVI and F-NZVI placed on unsaturated porous media

MIH capabilities of F-NZVI, both as free-foam and foam placed onto unsaturated porous media, under applied LF-EMF was investigated. The former provided a basic understanding of how much heat-free F-NZVI can be induced magnetically while the latter more realistically indicated the MIH of F-NZVI for vadose zone remediation. This is because when applied for remediation, F-NZVI will be injected to flush VOCs (Zhao et al., 2016; Maire and Fatin-Rouge, 2017) while leaving behind the NZVI in the vadose zone, where it helps generate heat under applied LF-EMF.

For the free-foam MIH experiments, a 25-mL screw-cap glass vial containing 12.5 mL of F-NZVI sample, generated under the optimal conditions, was placed into the center of the induction coil of a custom-made electromagnetic field generator (EMFG) (Fig. S3). The EMFG produced the LF-EMF at a current density of 13 A and a frequency of 150 kHz. The glass vial was inserted into an insulator prior to the MIH study. An infrared and contact thermometer (Fluke 561, Everett, Washington) was utilized to monitor the temperature changes from the induced heat. The induced temperature under the applied LF-EMF was monitored at 5, 10, and 15 min. Each experiment was performed in duplicate. In addition to the F-NZVI, the NZVI in DI water and in a SLES suspension (not foam) at a particle concentration of 50 g/L was also evaluated for MIH capabilities in order to be compared with F-NZVI to determine if employing foam as a vehicle to carry NZVI promotes or retards MIH. The MIH

capabilities of each NZVI-carrying vehicle (DI water, SLES dispersion, and SLES foam) was defined as the temperature change (ΔT) with respect to the amount of NZVI (g).

For the placed F-NZVI, the same experimental setup as described in Section 2.3 was used to generate and deliver F-NZVI (with 50 g/L of initial NZVI suspension) through an unsaturated porous media column. 60 PVs of F-NZVI were injected via up-flow mode to place the NZVI in the column. Then, the sand with the NZVI placement was dissected into eight 2-cm long segments followed by placing each segment onto the induction coil supplying the LF-EMF at a frequency of 150 kHz and current density of 13 A for 15 min, and the temperature was then recorded. The same experiment, except generating F-NZVI using 100 g/L NZVI in 3% SLES (w/w), was also carried out to evaluate the effect of a higher deposited NZVI concentration on ΔT in the unsaturated porous media.

2.5. Enhanced TCE evaporation by F-NZVI with MIH

F-NZVI coupled with MIH was investigated for its capabilities of enhancing TCE evaporation in a batch study. The 25-ml glass vial in this experiment contained 2 mL of F-NZVI (generated using the optimal condition, i.e., 100 g/L NZVI in 3% (w/w) SLES and a 500 mL/min N_2 rate) and 17.20 g of quartz sand with three different water saturations (WS) (5%, 25%, and 50%) to establish the role of water saturation on enhanced TCE evaporation via F-NZVI and MIH. A pure phase TCE of 0.25 mL (or 3.5% saturation) was pipetted into the vial prior to being promptly capped with Teflon Mininert™ to prevent TCE gas leaving the reactor. The reactor was homogenized in an orbital shaker for 30 min prior to the study. Control reactors, including TCE in sand without F-NZVI, were created via the same setup with the same three WS. The vial was insulated and placed into the center of the induction coil of a custom-made EMFG (see SI) at 13 A and 150 kHz for the MIH study for 5, 10, 15, 30, and 60 min in order to evaluate enhanced TCE evaporation kinetics. The temperature was measured using an infrared and a contact thermometer. The magnitude of the applied electric field (|E| with units of V/m) generated by the EMFG was determined by recording the voltage at different distances from the center of the induction coil (Fig. S3 in SI). The amount of TCE evaporation based on F-NZVI being coupled with MIH was quantified by sampling 50 μL of headspace via a gastight syringe through the Teflon Mininert™ valve. The gas sample was analyzed for the concentrations of TCE and its chlorinated byproducts with a 20 m Agilent J & W DB-624 capillary column on an Agilent 7820GC/ECD with appropriate calibration. The TCE evaporation in the reactor with F-NZVI, but without LF-EMF, was also monitored for the sake of comparison.

3. Results and discussion

3.1. Optimal condition for F-NZVI generation

As previously reported in the literature (Shen et al., 2011; Ding et al., 2013), SLES successfully generated foam (Fig. 1a) and F-NZVI (Fig. 1b). The quality of the foam (see Eq. S-1 in SI) was very high, both with (99.66%–99.84%) and without NZVI (99.76%–99.97%), for all experimental conditions. Fig. 1c illustrates the bubble size distribution of F-NZVI at SLES 3% (w/w) and a N_2 flow rate of 500 mL/min, i.e., the optimal condition. Most of the F-NZVI population had bubble sizes between 6 and 10 μm. Under this optimal condition, the F-NZVI half-life ($t_{1/2}$) was 170 ± 3.50 min (Fig. S4) while it contained 33.49 ± 3.72 g/L of NZVI when begun with an initial NZVI concentration of 50 g/L (Fig. 1d). The capability of F-NZVI at this optimal condition to carry NZVI was equivalent to 67% of the NZVI stock solution. Consequently, this ideal F-NZVI formation was used for all experiments that followed unless otherwise specified.

It should be noted that adding NZVI to the foam did not significantly alter foam stability, i.e., for the optimal condition, $t_{1/2} = 173 \pm 2.90$ and 170 ± 3.50 min for the control SLES foam without NZVI and F-NZVI, respectively (Fig. S4). Similarly, bubble size distributions between the SLES foam without NZVI and the F-NZVI were quite similar (Fig. 1c). This common synergetic effect of nanoparticles and surfactant in foam stabilization has previously been documented (Binks et al., 2008; Lv et al., 2015). As can be seen in Fig. 1b, a micrograph of F-NZVI at 50 g/L in 3% (w/w) SLES in 500 mL/min N_2 depicts the black aggregates of SLES-modified NZVI being sorbed onto the surface of the foam bubble between the contact line of the two phases (gas and liquid). The accumulation of SLES-modified NZVI on the foam surface is similar to the interfacial targeting of the NAPL source zone by amphiphilic polymer-modified NZVI in saturated porous media reported in recent studies (Saleh et al., 2005; Phenrat et al., 2011b; Phenrat and Kumloet, 2016). The film of attached SLES-modified NZVI onto the foam bubble may increase the surface elasticity of the foam, which subsequently enhances foam stability. Recent research has revealed that aggregates of nanoparticles at the gas–liquid interface can form “colloidal armor”, elevating dilational elasticity and thereby stabilizing foam against coarsening (exchange of gas between bubbles based on differences in Laplace pressure) (Stocco et al., 2009).

3.2. Delivery and placement of F-NZVI onto an unsaturated sand-packed column

Fig. 2a illustrates the breakthrough curve of F-NZVI generated at the optimal condition (50 g/L NZVI stock solution in 3% (w/w) SLES at a 500 mL/min N_2 flow rate). The foam quality of F-NZVI entering the sand-packed column was 99.83%, with the liquid portion of the foam (0.17%) carrying 41.32 g/L of NZVI. Noticeably, from the 5th PV to the 20th PV, the breakthrough NZVI concentrations seemed to reach a steady state around 45% of the influent concentration. The unsaturated media filtered around half of the NZVI carried by the foam. During the initial state of F-NZVI delivery, the unsaturated sand-packed column had low water saturation (3.04 ± 0.35% PV) and the initial capillary pressure in the medium was greater than the critical capillary pressure of the foam destruction, $P_{cr\text{-}foam}$ (Saiers and Lenhart, 2003; Zhong et al., 2010). This promoted bubble rupture, which resulted in deposition of the NZVI on the sand grain (Saiers and Lenhart, 2003; Zhong et al., 2010), as experimentally observed. This finding is in robust agreement with a recent study that reported NZVI (3 g/L) carried by the foam generated by SLES (0.5% (w/w)) was filtered at approximately 40% by an unsaturated sand-packed column (grain diameter of 0.45–0.6 mm) (Ding et al., 2013). Presumably, the work presented here generated foam at a higher NZVI concentration than Ding's group, which caused more agglomeration of NZVI in the foam (see NZVI agglomerates attached on F-NZVI in Fig. 1b) and thus was more easily filtered out by the unsaturated porous media.

Nevertheless, from the 20th to the 60th PV, the breakthrough NZVI concentrations gradually increased to be more than 100% transportability through the unsaturated packed bed, suggesting re-entrainment of the deposited NZVI. Although we did not visually observe flooding of the unsaturated sand-packed column during the 60-PV injection of F-NZVI (see the clips, SC1 and SC2, portraying SLES foam and F-NZVI generation as well as transport through the unsaturated sand-packed column in SI), after the 20th PV, it was entirely possible that the liquid from the foam rupture may have accumulated in the lower portion of the unsaturated sand-packed column and exceeded the critical moisture content (θ_{cr}). At this critical moisture content, the capillary pressure of the porous

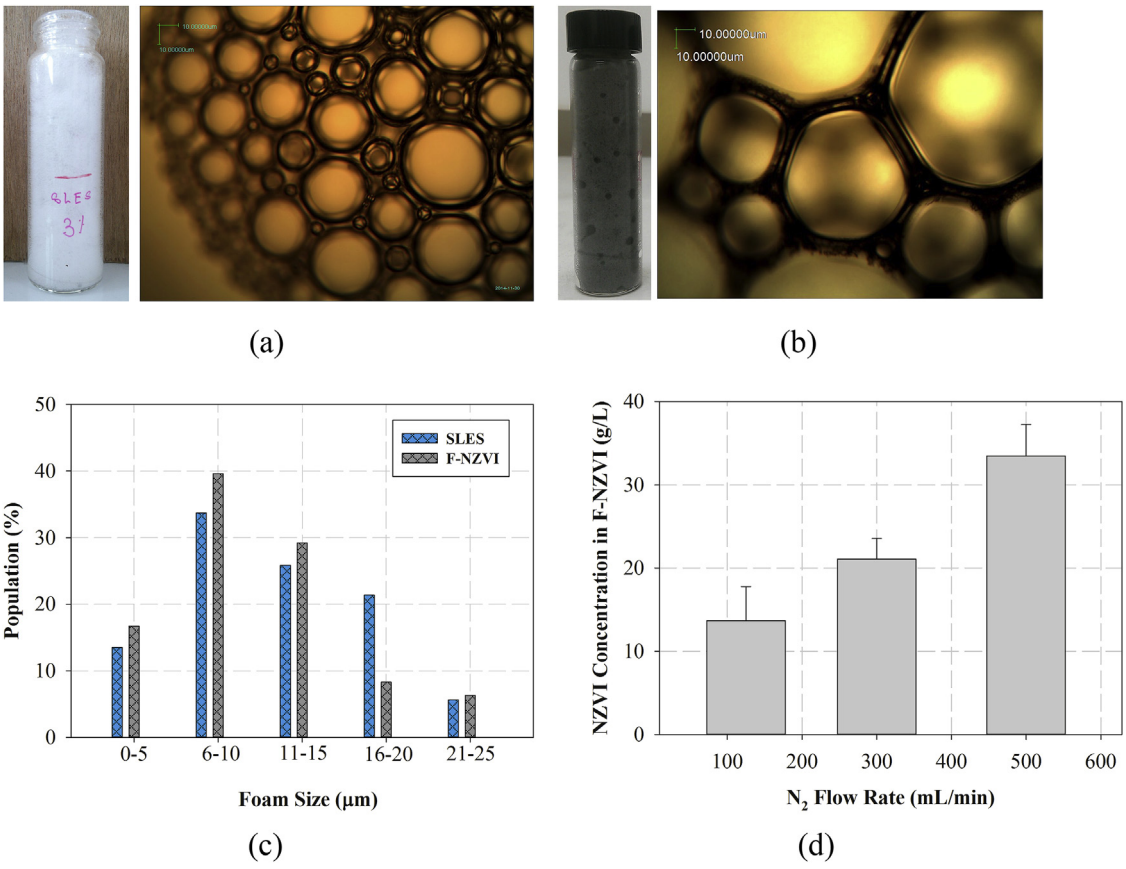

Fig. 1. Micrographs of: (a) SLES foam without NZVI in 3% SLES at 500 mL/min N_2 and (b) F-NZVI under the optimal condition containing 33.49 ± 3.72 g/L NZVI in 3% SLES at 500 mL/min N_2; focus is on NZVI aggregates formed on the bubble surface. (c) Bubble size distributions of SLES foam without NZVI and optimal F-NZVI. (d) NZVI carrying capacity (g/L) of F-NZVI at various N_2 flow rates, including the optimal flow rate (500 mL/min).

medium decreased to below the $P_{cr\text{-}foam}$; thus, this would have resulted in less foam rupture as along with regeneration of the foam from the pore liquid which can detach deposited NZVI from the unsaturated sand grain. These phenomena enhanced F-NZVI mobility through the unsaturated sand-packed column. This interesting behavior was not observed in Ding's study, where a transport experiment was conducted up to only 2 PVs (Ding et al., 2013). Potentially, the moisture content of the unsaturated sand media in their research might not have arrived at the critical point. Nevertheless, it is worth highlighting that, typically, θ_{cr} is from 10% to 20% PV (Saiers and Lenhart, 2003). Consequently, the accumulation of liquid to reach θ_{cr} at the location close to the foam injection point should not significantly result in any unintended vertical percolation of DNAPL in the underlying groundwater (Jeong et al., 2000).

Supplementary video related to this article can be found at

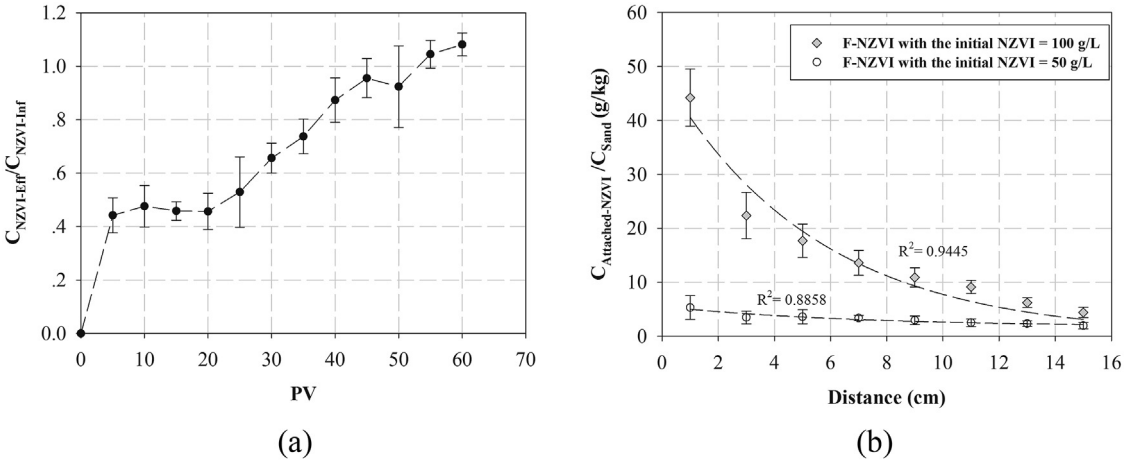

Fig. 2. (a) Breakthrough curve of F-NZVI at the initial NZVI concentration of 50 g/L over 60-PV delivery through an unsaturated sand-packed column and (b) the placed NZVI profile along the unsaturated sand-packed bed for 60-PV delivery of F-NZVI generated using the initial NZVI concentrations of 50 and 100 g/L in 3% (w/w) SLES stock solution and a N_2 flow rate of 500 mL/min.

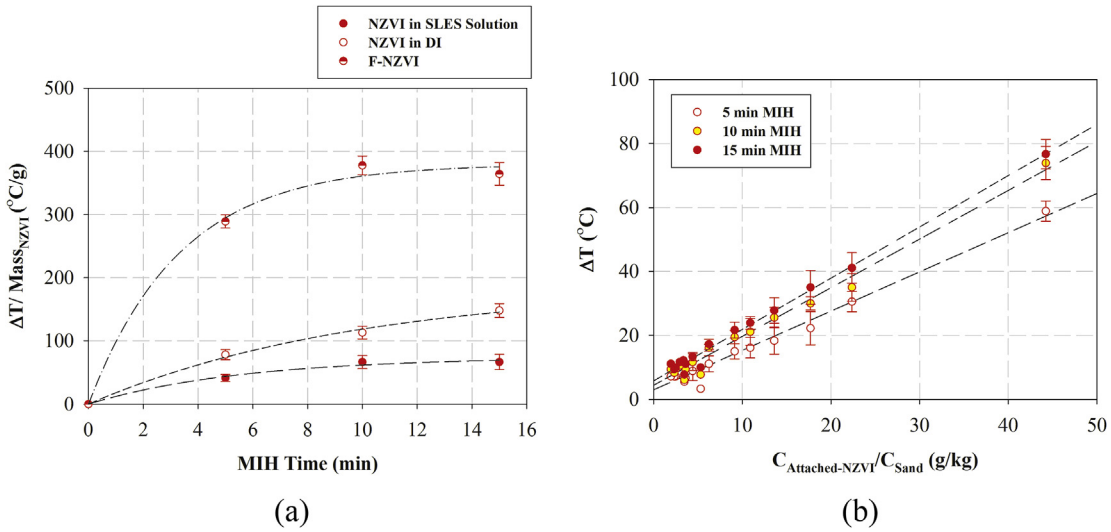

Fig. 3. (a) MIH kinetics of F-NZVI compared to NZVI in DI water and SLES concentration (3% (w/w)) and (b) linear trend between deposited NZVI concentration ($C_{Attached}$-NZVI/C_{Sand} (g/kg)) and induced ΔT (°C) at 5, 10, and 15 min MIH under 150 kHz and 13 A LF-EMF.

http://dx.doi.org/10.1016/j.chemosphere.2017.05.114.

Fig. 2b shows the NZVI attached to the sand in the unsaturated packed column after the 60-PV delivery of F-NZVI at the initial NZVI concentrations of 50 and 100 g/L. The concentration of NZVI deposited on the sand diminished exponentially with the distance from the inlet, in line with typical infiltration behavior of colloidal and nanoparticles in unsaturated porous media (Ding et al., 2013). However, the amount of deposited NZVI in this study was greater than previous investigations by approximately 10- to 100-fold because the initial NZVI concentrations in the liquid portion of the F-NZVI here were 50 and 100 g/L, while the NZVI concentration in the foam used earlier was only up to 4.4 g/L (Ding et al., 2013). We designed the NZVI placement in the unsaturated porous media to achieve high particle concentrations as the greater the placed NZVI, the more effective the thermally-enhanced evaporation of TCE promoted by NZVI under LF-EMF.

Overall, the F-NZVI synthesized in this study can be delivered through the unsaturated porous media and can be placed at significant NZVI concentrations for the purposes of vadose zone remediation.

3.3. MIH rate of F-NZVI

3.3.1. Free F-NZVI

NZVI is a ferromagnetic material with $\Delta U = 6.7 \times 10^4$ emu G/g, as confirmed by the VSM results in Fig. S5 as well as in a detailed discussion of the results in the SI (Phenrat and Kumloet, 2016; Phenrat et al., 2016). Under applied LF-EMF, the DI, SLES solution, and SLES foam control samples without NZVI could not generate any heat. However, DI and SLES solutions with NZVI as well as the F-NZVI-generated heat substantially raised the temperature of the suspension, just as expected (Fig. 3a). For all cases, ΔT per unit mass of NZVI ($Mass_{NZVI}$) was above 65 °C/g for 15 min. However, their heat induction rate constant (k_{HI}) (determined from Eq. (2)) and maximum induced temperature increase ($\Delta T_{max}/Mass_{NZVI}$) significantly depended on their vehicles.

$$\frac{\Delta T}{Mass_{NZVI}} = \frac{\Delta T_{Max}}{Mass_{NZVI}}\left(1 - e^{-k_H t}\right) \quad (2)$$

Intriguingly, F-NZVI ($K_{HI} = 29.94 \times 10^{-2}$ min^{-1} and $\Delta T_{max}/Mass_{NZVI} = 380$ °C/g) was the fastest in terms of heating kinetics, followed by NZVI in SLES solution ($K_{HI} = 17.88 \times 10^{-2}$ min^{-1} and $\Delta T_{max}/Mass_{NZVI} = 74$ °C/g), and NZVI in DI water ($K_{HI} = 10.14 \times 10^{-2}$ min^{-1} and $\Delta T_{max}/Mass_{NZVI} = 186$ °C/g). Of note, the K_{HI} of NZVI in DI water in the present study was similar to that reported previously (Phenrat et al., 2016). The difference of K_{HI} and $\Delta T_{max}/Mass_{NZVI}$ generated by NZVI in the three different vehicles may be attributed to the specific heat capacity (C_P) of each carrying media. As for the DI water, SLES solution, and F-NZVI examined herein, they contained the same type of NZVI with $\Delta U = 6.7 \times 10^4$ emu G/g, and the heat dissipation per unit of NZVI mass should have been the same under exactly the same LF-EMF if the carrying media did not play any role. Nonetheless, the heat dissipated to mostly air in the foam structure of F-NZVI (air = 99.83%) while the same amount of heat dissipated to water in the DI water sample and to 3% (w/w) SLES in the SLES solution sample. As the C_P of air (1.012 J/g/C at 25 °C) is lower than the C_P of DI water (4.1813 J/g/C at 25 °C) by roughly a factor of 4, it is comprehensible that the K_{HI} of the F-NZVI was three-fold greater than that of NZVI in the DI water. Likewise, the ionic surfactant is known to decrease the C_P of an aqueous solution at concentrations greater than the critical micelle concentration (CMC) (Kresheck, 2006). For this reason, at 3% (w/w) SLES, which is greater than its CMC, the C_P of the SLES solution is supposed to be lower than that of DI, leading to faster heating kinetics and extent of NZVI in SLES solution versus DI as observed in this study. Yet, the decreased C_P of 3% (w/w) SLES concentration may still be larger than that of air in F-NZVI; this helps clarify the poorer heating kinetics of NZVI in SLES solution in comparison to that of F-NZVI.

3.3.2. F-NZVI placed on an unsaturated porous media

Without F-NZVI, unsaturated sand with and without the SLES foam under LF-EMF could not generate any measurable heat. On the other hand, F-NZVI placed onto the unsaturated sand could, in fact, produce heat and raise the temperature under an applied LF-EMF, though the temperature increase was significantly lower than that of free F-NZVI based on the same foam generating conditions. For example, Fig. S6(a) shows the ΔT for F-NZVI (generated at the initial NZVI concentration of 50 g/L) deposited onto the unsaturated sand at each distance from the inlet according to the NZVI emplacement profile in Fig. 2b. It is noteworthy that the F-NZVI placement profile in Fig. S6(a) was generated under the same conditions as the free F-NZVI emplacement profile in Fig. 3a. MIH

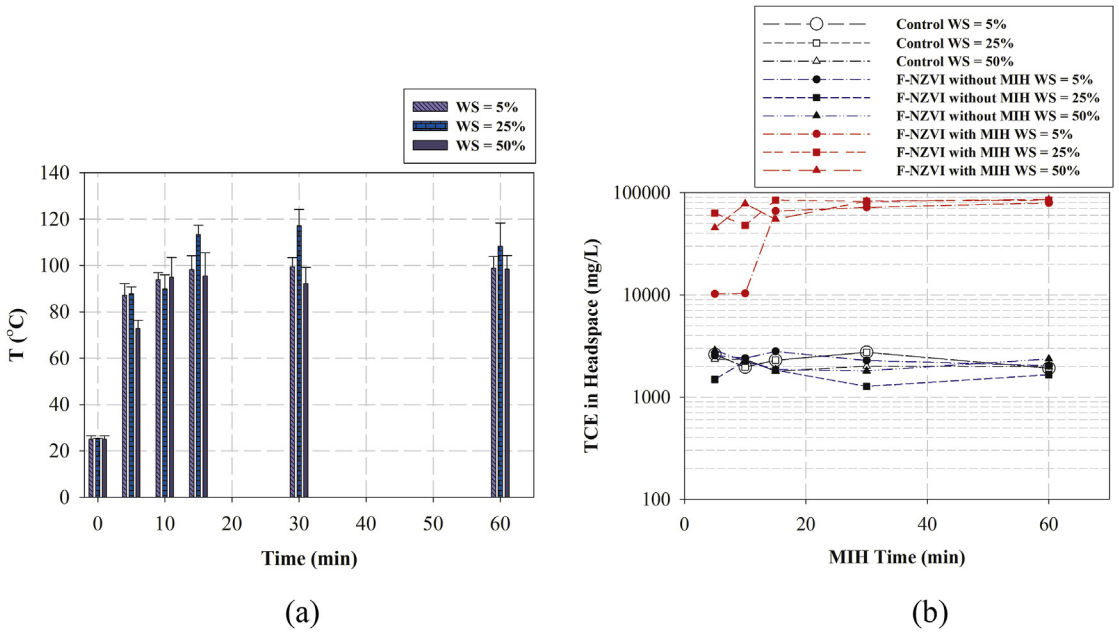

Fig. 4. (a) Heating kinetics of reactors containing unsaturated sand at WS = 5, 25, and 50% and TCE saturation = 3.5% induced by F-NZVI under 150 kHz and 13 A and (b) kinetics of TCE evaporation to headspace with and without applied LF-EMF and as a function of MIH duration.

was conducted for 5, 10, and 15 min for each sand segment. As observed in Fig. S6(a), for each segment, the induced ΔT slightly rose with time from 5 to 15 min. Nevertheless, ΔT ranged only from 3 °C to 11 °C, which is insufficient for the application of thermally-enhanced remediation. The much lower ΔT of deposited F-NZVI in the unsaturated porous media compared to free-foam was probably a consequence of the low NZVI concentration attached to the unsaturated sand. For example, the maximum attached NZVI concentration from the deposition of the F-NZVI at the initial NZVI concentration of 50 g/L, according to Fig. 2b, was only around 5 g/kg while the NZVI concentration in the free F-NZVI was 41.32 g/L. To achieve meaningful thermally-enhanced vadose zone remediation, ΔT greater than 40 °C is preferable. This can be accomplished using the F-NZVI foam with the initial NZVI concentration of 100 g/L in 3% (w/w) SLES stock solution and a N_2 flow rate of 500 mL/min. The induced ΔT from the NZVI deposition with this condition substantially increased with time, i.e., 41 °C and 77 °C for the placed NZVI concentrations of 22 g/kg and 44 g/kg for MIH of 5–15 min, respectively (Fig. S6(b) in comparison to Fig. S6(a)).

Intuitively, at a particular MIH time point, the greater the placed NZVI, the higher the increased ΔT, just as illustrated in Fig. 3b (derived from ΔT from Figs. S6(a) and (b) and the mass of deposited NZVI in Fig. 2b). This finding suggests that delivery of the F-NZVI at the initial NZVI concentration of 100 g/L should place the NZVI at the deposited concentration of 22–44 g/kg, adequate for inducing ΔT up to 77 °C for thermally-enhanced vadose remediation.

3.4. Enhanced TCE volatilization by F-NZVI under LF-EMF

Here, we evaluated the feasibility of thermally-enhanced TCE volatilization using MIH of the F-NZVI deposited onto the unsaturated porous media at the attached NZVI concentration of 44 g/kg, described in the previous section. The control reactors (i.e., unsaturated sand with water saturation (WS) = 5, 25, and 50% and TCE (pure phase) saturation = 3.5% without the F-NZVI) and the reactors with F-NZVI but without MIH could not generate any measurable heat, and the temperature remained at 25 °C for 60 min. However, under an applied LF-EMF, the deposited F-NZVI generated heat to achieve temperatures from 95 °C to 110 °C (ΔT from 70 °C to 85 °C) in 15 min (Fig. 4a). Moreover, the WS in the unsaturated porous media did not obviously affect the heating kinetics of the F-NZVI reactors in the LF-EMF. Hence, the deposited F-NZVI concentration was the main governing factor.

As theoretically hypothesized, the heat generated by F-NZVI under LF-EMF substantially enhanced TCE volatilization in the batch reactors. As depicted in Fig. 4b (presented in log scale), TCE concentrations in the headspace of the control reactors and F-NZVI reactors without LF-EMF application were relatively constant over 60 min, i.e., 2236 ± 329 mg/L and 2114 ± 465 mg/L, respectively. Additionally, WS did not appear to play any evident role in TCE volatilization within these reactors. However, TCE concentrations in the headspace of F-NZVI reactors with MIH rose sharply from 0 to 5 min MIH for WS = 25% and 50%, while it increased more gradually in the reactor with WS = 5%. After nearly 15 min of MIH, the TCE concentration in the headspace of all MIH reactors reached a similar maximum concentration of 81,504 ± 4751 mg/L, regardless of the WS. Obviously, thermally-enhanced TCE volatilization was visually observed (see the clip, SC3, exhibiting thermally-enhanced TCE volatilization in the SI). Consequently, the MIH of F-NZVI deposited in the unsaturated porous media at a NZVI concentration of 44 g/kg elevated TCE volatilization by 39.51 ± 6.59-fold compared to reactors without MIH.

Supplementary video related to this article can be found at http://dx.doi.org/10.1016/j.chemosphere.2017.05.114.

3.5. Comparative analysis of the theoretical performance of MIH with F-NZVI and RFH without F-NZVI

This study featured a proof-of-concept experiment for using F-NZVI together with LF-EMF to thermally enhance VOC removal in the vadose zone when combined with SVE or soil flushing. Several unique features were experimentally uncovered. Nevertheless, the benefit of F-NZVI together with LF-EMF may be more pronounced once we theoretically compare the performance of LF-EMF with NZVI to that of LF-EMH EMF and RFH without F-NZVI. Both LF-EMF and RFH are forms of electromagnetic heating; the only difference

is their frequencies, as discussed in the Introduction. For the application of F-NZVI with LF-EMF in the unsaturated porous media discussed previously, the ΔT was 77 °C. Given that air C_P is 1.006 kJ/kg K, air density is 1.184 kg/m^3, the reactor volume was 1.5×10^{-5} m^3, and the heating time was 5 min, we estimated the theoretical amount of power dissipated by MIH (P_{MIH}) of F-NZVI equal to 4.59×10^{-3} W.

However, under LF-EMF of 150 kHz and I = 13 A, causing |E| = 79.88 V/m (Fig. S7 in SI), even without F-NZVI, EMF would interact with the sand grain to create heat via conduction and dielectric loss, but not magnetic loss. We estimated the theoretical amount of power dissipated by EM heating, P_{EM} (W) without F-NZVI, using:

$$P_{EM} = V2\pi f \varepsilon_0 \varepsilon''_{eff} |E|^2, \quad (3)$$

where V was the volume of the reactor, |E| was the magnitude of the applied electric field (V/m), f was the irradiated frequency (1/s), ε_0 was the permittivity of free space (8.85×10^{-12} F/m), and ε''_{eff} was an effective imaginary permittivity (unit less) that was a function of f (Revil, 2013). Given that |E| = 79.88 V/m, as measured from LF-EMF (see Fig. S7 in SI), $\varepsilon''_{eff} = 39.81$ for $f = 150$ kHz (Revil, 2013), and the reactor volume was 1.5×10^{-5} m^3; therefore, the irradiated frequency of 150 kHz yielded $P_{EM} = 3.18 \times 10^{-5}$ W. This low value of P_{EM} agreed with the experimental results previously discussed such that when applying LF-EMF to the unsaturated sand without F-NZVI, measurable heat was not generated. Thus, using F-NZVI together with LF-EMF can induce heat 145-fold greater than that via LF-EMF without F-NZVI.

In a similar way, we could theoretically calculate the frequency of RFH necessary to produce the same theoretical amount of power dissipation obtained from P_{MIH}. Furthermore, RFH is a form of EM heating that can be estimated using Eq. (3) (referred to as the theoretical amount of power dissipated by RFH (P_{RFH})). Given $\varepsilon''_{eff} = 15.85$ for $f = 54.5$ MHz (Revil, 2013), the irradiated frequency of RFH to yield $P_{RFH} = 4.59 \times 10^{-3}$ W, equivalent to the P_{MIH}, is 54.5 MHz. This is in line with the irradiation frequency typically used in RFH remediation (500 kHz–500 MHz) (Lowe et al., 1999; Price et al., 1999). Noticeably, the irradiated frequency of RFH was approximately 363-fold greater than that required by LF-EMF when applied with F-NZVI. This indicated that using F-NZVI together with LF-EMF could theoretically be an alternative to RFH because it does not necessitate as high an irradiation frequency as RFH and should still lead to both lower capital and operational costs versus RFH because the electrical transmission losses and capital costs of RFH equipment rise with the frequency of EMF (Vermeulen and McGee, 2000).

Using F-NZVI for this enhanced technique requires an extra cost of NZVI in comparison to LF-EMH or RFH. However, the additional material cost is in the same range as using NZVI for saturated zone remediation. For example, for one cubic meter of vadose zone remediation, given a porosity of 0.33 and foam quality of 99.84% (i.e., 99.84% air and 0.16% NZVI dispersion), only 0.053 kg of NZVI would be needed for 1 PV of F-NZVI injection. Even for 60 PVs to deposit enough NZVI to generate heat under LF-EMF to 77 °C, only 3.16 kg of NZVI is necessary. This is in concurrence with NZVI mass required for saturated zone remediation. In general, the NZVI concentration for saturated zone remediation is from 1 to 20 g/L (Phenrat et al., 2010a). Thus, for one PV injection (one cubic meter), the mass for NZVI injection is between 0.33 and 6.6 kg (for a NZVI concentration of 1–20 g/L). Therefore, the material cost of F-NZVI for this application should not be prohibitive.

Although this study demonstrates the feasibility of using F-NZVI together with LF-EMF to thermally enhance VOC removal in a vadose zone, several aspects of this novel technique need further investigation to make this concept truly applicable. For example, when F-NZVI deposits NZVI in the vadose zone, NZVI oxidation by O_2 is unavoidable. Oxidation will transform ferromagnetic NZVI to ferrimagnetic magnetite and maghemite (Phenrat et al., 2007, 2009a), presumably reducing MIH capabilities. Hence, understanding the life time and degree of NZVI transformation, as well as the decrease of MIH from oxidation, is imperative. Similar to RFH, further investigation into a field-scaled LF-EMF generator, a matching network, operating frequency, power level, antenna, applicator length, number of applicators, applicator position and orientation, mutual coupling between applicators, electrical phasing, and soil properties is essential for field-scale design (Price et al., 1999).

Acknowledgement

This research was funded in part by: (1) the Thailand Research Fund (TRF) (MRG5680129), (2) the National Nanotechnology Center, a member of the National Science and Technology Development Agency, through grant number P-11-00989, and (3) the National Research Council (R2556B070).

Appendix A. Supplementary data

Supplementary data related to this article can be found at http://dx.doi.org/10.1016/j.chemosphere.2017.05.114.

References

Abreu, L.D.V., Johnson, P.C., 2005. Effect of vapor source–building separation and building construction on soil vapor intrusion as studied with a three-dimensional numerical model. Environ. Sci. Technol. 39, 4550–4561.
Berge, N.D., Ramsburg, C.A., 2010. Iron-mediated trichloroethene reduction within nonaqueous phase liquid. J. Contam. Hydrol. 118, 105–116.
Beyke, G., Fleming, D., 2005. In situ thermal remediation of DNAPL and LNAPL using electrical resistance heating. Remediat. J. Summer 5–22.
Binks, B.P., Kirkland, M., Rodrigues, J.A., 2008. Origin of stabilisation of aqueous foams in nanoparticle–surfactant mixtures. Soft Matter 4, 2373–2382.
Boulding, J.R., Ginn, J.S., 2003. Practical Handbook of Soil, Vadose Zone, and Ground-Water Contamination: Assessment, Prevention, and Remediation. CRC Press, New York.
Brusseau, M.L., Carroll, K.C., Truex, M.J., Becker, D.J., 2013. Characterization and remediation of chlorinated volatile organic contaminants in the vadose zone: an overview of issues and approaches. Vadose Zone J. 12.
Ding, Y., Liu, B., Shen, X., Zhong, L., Li, X., 2013. Foam-assisted delivery of nanoscale zero valent iron in porous media. J. Environ. Eng. 139, 1206–1212.
Falciglia, P.P., Urso, G., Vagliasindi, F.G.A., 2013. Microwave heating remediation of soils contaminated with diesel fuel. J. Soils Sediments 13, 1396–1407.
He, F., Zhao, D., Liu, J., Roberts, C.B., 2007. Stabilization of Fe-Pd nanoparticles with sodium carboxymethyl cellulose for enhanced transport and dechlorination of trichloroethylene in soil and groundwater. Ind. Eng. Chem. Res. 46, 29–34.
He, F., Zhao, D., Paul, C., 2010. Field assessment of carboxymethyl cellulose stabilized iron nanoparticles for in situ destruction of chlorinated solvents in source zones. Water Res. 44, 2360–2370.
Heron, G., Van Zutphen, M., Christensen, T.H., Enfield, G.C., 1998. Soil heating for enhanced remediation of chlorinated solvents: a laboratory study on resistive heating and vapor extraction in a silty, low-permeable soil contaminated with trichloroethylene. Environ. Sci. Technol. 32, 1474–1481.
Jeong, S.-W., Corapcioglu, M.Y., Roosevelt, E.W., 2000. Micromodel study of surfactant foam remediation of residual trichloroethylene. Environ. Sci. Technol. 34, 3456–3461.
Kocur, C.M., Lomheim, L., Boparai, H.K., Chowdhury, A.I., Weber, K.P., Austrins, L.M., Edwards, E.A., Sleep, B.E., O'Carroll, D.M., 2015. Contributions of abiotic and biotic dechlorination following carboxymethyl cellulose stabilized nanoscale zero valent iron injection. Environ. Sci. Technol. 49, 8648–8656.
Kresheck, G.C., 2006. The temperature dependence of the heat capacity change for micellization of nonionic surfactants. J. Colloid Inrterface Sci. 298, 432–440.
Li, Z., Kawashita, M., Araki, N., Mitsumori, M., Hiraoka, M., Doi, M., 2010. Magnetite nanoparticles with high heating efficiencies for application in the hyperthermia of cancer. Mater. Sci. Eng. C 30, 990–996.
Liang, L., Guan, X., Shi, Z., Li, J., Wu, Y., Tratnyek, P.G., 2014a. Coupled effects of aging and weak magnetic fields on sequestration of selenite by zero-valent iron. Environ. Sci. Technol. 48, 6326–6334.
Liang, L., Sun, W., Guan, X., Huang, Y., Choi, W., Bao, H., Li, L., Jiang, Z., 2014b. Weak

magnetic field significantly enhances selenite removal kinetics by zero valent iron. Water Res. 49, 371–380.
Lowe, D.F., Oubre, C.L., Ward, C.H., 1999. Soil Vapor Extraction Using Radio Frequency Heating: Resource Manual and Technology Demonstration. CRC Press, New York.
Lv, Q., Li, Z., Li, B., Li, S., Sun, Q., 2015. Study of nanoparticle–surfactant-stabilized foam as a fracturing fluid. Ind. Eng. Chem. Res. 54, 9468–9477.
Maire, J., Fatin-Rouge, N., 2017. Surfactant foam flushing for in situ removal of DNAPLs in shallow soils. J. Hazard. Mater. 321, 247–255.
Mulligan, C.N., Eftekhari, F., 2003. Remediation with surfactant foam of PCP-contaminated soil. Eng. Geol. 70, 269–279.
Nakamura, T., Senior, C.L., Burns, E.G., Bell, M.D., 2000. Solar-powered soil vapor extraction for removal of dense nonaqueous phase organics from soil. J. Environ. Sci. Health A Tox. Hazard. Subst. Environ. Eng. 35, 795–816.
O'Carroll, D.M., Sleep, B., Krol, M., Boparai, H., Kocur, C., 2013. Nanoscale zero valent iron and bimetallic particles for contaminated site remediation. Adv. Water Resour. 51, 104–122.
Phenrat, T., Kumloet, I., 2016. Electromagnetic induction of nanoscale zerovalent iron particles accelerates the degradation of chlorinated dense non-aqueous phase liquid: proof of concept. Water Res. 107, 19–28.
Phenrat, T., Saleh, N., Sirk, K., Tilton, R.D., Lowry, G.V., 2007. Aggregation and sedimentation of aqueous nanoscale zerovalent iron dispersions. Environ. Sci. Technol. 41, 284–290.
Phenrat, T., Saleh, N., Sirk, K., Kim, H.-J., Tilton, R.D., Lowry, G.V., 2008. Stabilization of aqueous nanoscale zerovalent iron dispersions by anionic polyelectrolytes: adsorbed anionic polyelectrolyte layer properties and their effect on aggregation and sedimentation. J. Nanopart. Res. 10, 795–814.
Phenrat, T., Kim, H.-J., Fagerlund, F., Illangasekare, T., Tilton, R.D., Lowry, G.V., 2009a. Particle size distribution, concentration, and magnetic attraction affect transport of polymer-modified Fe^0 nanoparticles in sand columns. Environ. Sci. Technol. 43, 5079–5085.
Phenrat, T., Liu, Y., Tilton, R.D., Lowry, G.V., 2009b. Adsorbed polyelectrolyte coatings decrease Fe^0 nanoparticle reactivity with TCE in water: conceptual model and mechanisms. Environ. Sci. Technol. 43, 1507–1514.
Phenrat, T., Kim, H.-J., Fagerlund, F., Illangasekare, T., Lowry, G.V., 2010a. Empirical correlations to estimate agglomerate size and deposition during injection of a polyelectrolyte-modified Fe0 nanoparticle at high particle concentration in saturated sand. J. Contam. Hydrol. 118, 152–164.
Phenrat, T., Schoenfelder, D., Losi, M., Yi, J., Peck, S.A., Lowry, G.V., 2010b. Treatability study for a TCE contaminated area using nanoscale- and microscale-zerovalent iron particles: reactivity and reactive life time. In: Geiger, C.L., Carvalho-Knighton, K.M. (Eds.), Environmental Applications of Nanoscale and Microscale Reactive Metal Particles. American Chemical Society, Washington D.C, pp. 183–202.
Phenrat, T., Crimi, M., Illanagasekare, T., Lowry, G.V., 2011a. Reactive nanoparticles for the treatment of chlorinated dense nonaqueous phase liquids in soil and groundwater. In: Ram, M., Andreescu, E.S., Hanming, D. (Eds.), Nanotechnology for Environmental Decontamination. McGraw-Hill Publisher, New York, pp. 271–322.
Phenrat, T., Fagerlund, F., Illanagasekare, T., Lowry, G.V., Tilton, R.D., 2011b. Polymer-modified Fe0 nanoparticles target entrapped NAPL in two dimensional porous media: effect of particle concentration, NAPL saturation, and injection strategy. Environ. Sci. Technol. 45, 6102–6109.
Phenrat, T., Schoenfelder, D., Kirschling, T.L., Tilton, R.D., Lowry, G.V., 2015. Adsorbed poly(aspartate) coating limits the adverse effects of dissolved groundwater solutes on Fe0 nanoparticle reactivity with trichloroethylene. Environ. Sci. Pollut. Res. https://link.springer.com/article/10.1007/s11356-015-5092-4.
Phenrat, T., Thongboot, T., Lowry, G.V., 2016. Electromagnetic induction of zerovalent iron (ZVI) powder and nanoscale zerovalent iron (NZVI) particles enhances dechlorination of trichloroethylene in contaminated groundwater and soil: proof of concept. Environ. Sci. Technol. 50, 872–880.
Poppendieck, D.G., Loehr, R.C., Webster, M.T., 1999a. Predicting hydrocarbon removal from thermally enhanced soil vapor extraction systems. 1. Laboratory studies. J. Hazard. Mater. 69, 81–93.
Poppendieck, D.G., Loehr, R.C., Webster, M.T., 1999b. Predicting hydrocarbon removal from thermally enhanced soil vapor extraction systems: 2. Field study. J. Hazard. Mater. 69, 95–109.
Price, S.L., Kasevich, R.S., Johnson, M.A., Wiberg, D., Marley, M.C., 1999. Radio frequency heating for soil remediation. J. Air Waste Manag. Assoc. 49, 136–145.
Revil, A., 2013. Effective conductivity and permittivity of unsaturated porous materials in the frequency range 1 mHz–1GHz. Water Resour. Res. 49, 306–327.
Roland, U., Buchenhorst, D., Holzer, F., Kopinke, F.D., 2008. Engineering aspects of radio-wave heating for soil remediation and compatibility with biodegradation. Environ. Sci. Technol. 42, 1232–1237.
Ronen, D., Graber, E.R., Laor, Y., 2004. Volatile organic compounds in the saturated–unsaturated interface region of a contaminated phreatic aquifer. Vadose Zone J. 4, 337–344.
Rosenbloom, J., Mock, P., Lawson, P., Brown, J., Turin, H.J., 1993. Application of VLEACH to vadose zone transport of VOCs at an Arizona superfund site. Ground Water Monit. Remed. Summer 159–169.
Saiers, J.E., Lenhart, J.J., 2003. Colloid mobilization and transport within unsaturated porous media under transient-flow conditions. Water Resour. Res. 39, 1019.
Saleh, N., Phenrat, T., Sirk, K., Dufour, B., Ok, J., Sarbu, T., Matyjaszewski, K., Tilton, R.D., Lowry, G.V., 2005. Adsorbed triblock copolymers deliver reactive iron nanoparticles to the oil/water interface. Nano Lett. 5, 2489–2494.
Shen, X., Zhao, L., Ding, Y., Liu, B., Zeng, H., Zhong, L., Li, X., 2011. Foam, a promising vehicle to deliver nanoparticles for vadose zone remediation. J. Hazard. Mater. 186, 1773–1780.
Smith, L.A., Hinchee, R.E., 1993. In Situ Thermal Technologies for Site Remediation. CRC Press Inc., Boca Raton, Florida.
Soga, K., Kawabata, J., Kechavarzi, C., Coumoulos, H., Waduge, W., 2003. Centrifuge modeling of nonaqueous phase liquid movement and entrapment in unsaturated layered soils. J. Geotech. Geoenviron. Eng. 129, 173–182.
Stocco, A., Drenckhan, W., Rio, E., Langevin, D., Binks, B.P., 2009. Particle-stabilised foams: an interfacial study. Soft Matter 2215–2222.
Tratnyek, P.G., Johnson, R.L., 2006. Nanotechnologies for environmental cleanup. Nano Today 1, 44–48.
Truex, Michael J., Gillie, J.M., Powers, Jefferey G., Lynch, Kira P., 2009. Assessment of in situ thermal treatment for chlorinated organic source zones. Remediat. J. 19, 7–17.
Vermeulen, F., McGee, B., 2000. In-situ electromagnetic heating for hydrocarbon recovery and environmental remediation. J. Can. Petrol. Technol. 39, 25–29.
Wang, H., Chen, J., 2012. Enhanced flushing of polychlorinated biphenyls contaminated sands using surfactant foam: effect of partition coefficient and sweep efficiency. J. Environ. Sci. (China) 24, 1270–1277.
Wang, X., Chen, J., Lv, C., 2015. Evaluation of foam surfactant for foam-flushing technique in remediation of DDT-contaminated soil using data envelopment analysis method. Environ. Sci. Pollut. Res. 22, 2994–3003.
Werth, C.J., Reinhard, M., 1997. Effects of temperature on trichloroethylene desorption from silica gel and natural sediments. 2. Kinet. Environ. Sci. Technol. 31, 697–703.
Xu, C., Zhang, B., Wang, Y., Shao, Q., Zhou, W., Fan, D., Bandstra, J.Z., Shi, Z., Tratnyek, P.G., 2016. Effects of sulfidation, magnetization, and oxygenation on azo dye reduction by zerovalent iron. Environ. Sci. Technol. 50, 11879–11887.
Yang, J.-W., Cho, H.-J., Choi, G.-Y., Lee, S.-H., 2001. Cost-effective monitoring for a soil vapor extraction (SVE) system. A simplified modeling and gas sensor test. Environ. Monit. Assess. 70, 201–210.
Yoon, H., Valocchi, A.J., Werth, C.J., 2003. Modeling the influence of water content on soil vapor extraction. Vadose Zone J. 2, 368–381.
Zhao, Y.S., Su, Y., Lian, J.R., Wang, H.F., Li, L.L., Qin, C.Y., 2016. Insights on flow behavior of foam in unsaturated porous media during soil flushing. Water Environ. Res. 88, 2132–2141.
Zhong, L., Szecsody, J.E., Zhang, F., Mattigod, S.V., 2010. Foam delivery of amendments for vadose zone remediation: propagation performance in unsaturated sediments. Vadose Zone J. 9, 757–767.